Please cite this article in press as: Warias et al., tRNA Dissociation from EF-Tu after GTP Hydrolysis: Primary Steps and Antibiotic Inhibition, Biophysical Journal (2019), https://doi.org/10.1016/j.bpj.2019.10.028

Biophysical *Journal*
Article

Biophysical Society

# tRNA Dissociation from EF-Tu after GTP Hydrolysis: Primary Steps and Antibiotic Inhibition

Malte Warias,[1] Helmut Grubmüller,[1] and Lars V. Bock[1,*]
[1]Theoretical and Computational Biophysics, Max Planck Institute for Biophysical Chemistry, Göttingen, Germany

ABSTRACT In each round of ribosomal translation, the translational GTPase elongation factor Tu (EF-Tu) delivers a transfer RNA (tRNA) to the ribosome. After successful decoding, EF-Tu hydrolyzes GTP, which triggers a conformational change that ultimately results in the release of the tRNA from EF-Tu. To identify the primary steps of these conformational changes and how they are prevented by the antibiotic kirromycin, we employed all-atom explicit-solvent molecular dynamics simulations of the full ribosome-EF-Tu complex. Our results suggest that after GTP hydrolysis and $P_i$ release, the loss of interactions between the nucleotide and the switch 1 loop of EF-Tu allows domain D1 of EF-Tu to rotate relative to domains D2 and D3 and leads to an increased flexibility of the switch 1 loop. This rotation induces a closing of the D1-D3 interface and an opening of the D1-D2 interface. We propose that the opening of the D1-D2 interface, which binds the CCA tail of the tRNA, weakens the crucial EF-Tu-tRNA interactions, which lowers tRNA binding affinity, representing the first step of tRNA release. Kirromycin binds within the D1-D3 interface, sterically blocking its closure, but does not prevent hydrolysis. The resulting increased flexibility of switch 1 explains why it is not resolved in kirromycin-bound structures.

SIGNIFICANCE The protein elongation factor Tu (EF-Tu) delivers transfer RNAs (tRNAs) charged with amino acids to the translating ribosome, which synthesizes proteins. Here, based on recent structures and extensive computer simulations, we propose an atomistic mechanism of how GTP hydrolysis, triggered by successful binding of the correct tRNA, results in the rotation of a domain of EF-Tu, which opens the binding pocket of the 5′ end of the tRNA. Our results suggest that this opening weakens the interaction between EF-Tu and tRNA, a primary step toward dissociation from the tRNA, which is crucial for the continuation of protein synthesis. We find that the antibiotic kirromycin sterically blocks the domain rotation, thereby revealing the mechanism by which EF-Tu dissociation is prevented, stalling the synthesis of proteins.

## INTRODUCTION

Elongation factor Tu (EF-Tu) is a central part of the bacterial translation machinery. During each round of translation elongation, EF-Tu delivers an aminoacyl-tRNA (aa-tRNA) to the ribosome in a ternary complex with GTP (Fig. 1 *a*; (1)). The successful decoding of the messenger RNA codon by the aa-tRNA leads to a closing of the small ribosomal subunit (30S), which in turn docks EF-Tu at the sarcin-ricin loop of the large subunit (50S) in the GTPase-activated (GA) state (2,3). The transition of EF-Tu into a reorganized catalytic configuration in the GTPase-activated state catalyzes GTP hydrolysis to GDP (4,5), followed by the release of inorganic phosphate ($P_i$) and a conformational change of EF-Tu (6). Because the conformational change of EF-Tu occurs rapidly and its rate is limited by $P_i$ release, EF-Tu was suggested to behave like a "loaded spring" whose tension is relaxed after $P_i$ dissociation (6). This conformational change eventually leads to the transfer RNA (tRNA) being released from EF-Tu, followed by the accommodation of the tRNA into the A site and the dissociation of EF-Tu from the ribosome (7). Ensemble and single-molecule kinetic experiments indicate that EF-Tu dissociates first from the 3′ end of the tRNA and from the GTPase-associated center of the ribosome and subsequently from the rest of the tRNA (8). tRNA accommodation proceeds in a stepwise manner (9–12) via an intermediate elbow-accommodated conformation, and EF-Tu has been suggested to help the tRNA to assume an intermediate step before full accommodation (13).

*Submitted April 10, 2019, and accepted for publication October 22, 2019.*
*Correspondence: lbock@gwdg.de
Editor: Amedeo Caflisch.
https://doi.org/10.1016/j.bpj.2019.10.028

Please cite this article in press as: Warias et al., tRNA Dissociation from EF-Tu after GTP Hydrolysis: Primary Steps and Antibiotic Inhibition, Biophysical Journal (2019), https://doi.org/10.1016/j.bpj.2019.10.028



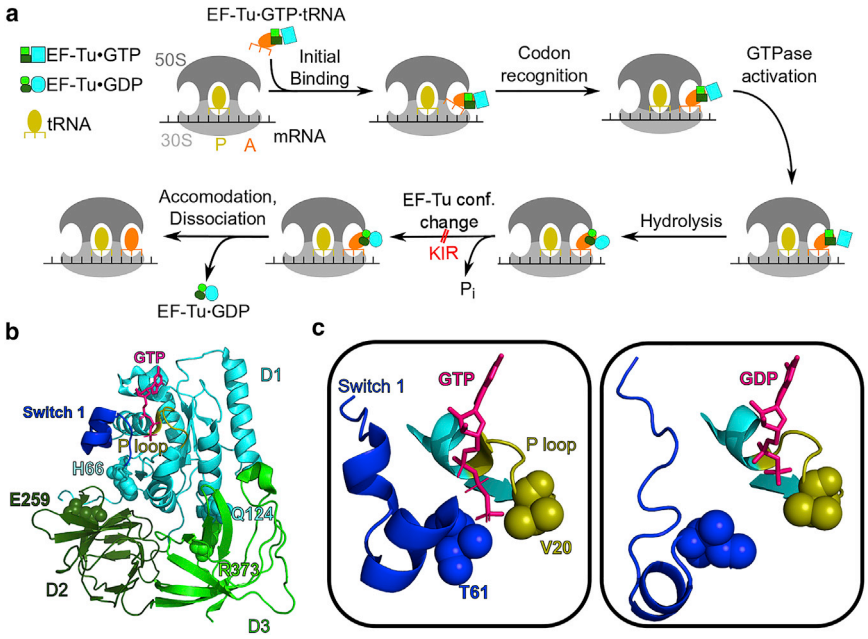


FIGURE 1 (*a*) Sketch of the mechanism by which EF-Tu delivers aa-tRNA to the ribosomal A site. EF-Tu is represented by three boxes (*light green*, *dark green*, *cyan*), and the aa-tRNA is shown in orange. (*b*) Cartoon representation of EF-Tu in the GTPase-activated conformation (3). Residues discussed in the text are shown as spheres, and GTP as sticks. (*c*) Switch 1 and P-loop are shown as cartoon representations for the GTPase-activated conformation and for a simulation snapshot containing GDP. The residues closest to the γ-phosphate of GTP are shown as spheres.

EF-Tu consists of the GTP-binding domain D1 and two β-barrel domains D2 and D3 (Fig. 1 *b*; (14)). All three domains bind the tRNA: the CCA tail of the tRNA along with the attached amino acid is bound to a cleft between D1 and D2, whereas D3 interacts with the T stem of the tRNA (15). A closed and an open conformation of the free ternary complex have been solved in complex with GTP and GDP, respectively (14,16). The main difference between the two conformations is a 100° rotation of D1 against D2 and D3 and a different fold of the switch 1 region, which is a part of D1. EF-Tu bound to the ribosome with nonhydrolyzable GTP (3,17) assumes a similar conformation as the isolated ternary complex (15). The switch 1 region was observed in an α-helical conformation for closed GTP-bound EF-Tu (14) and in a β-sheet conformation for open GDP-bound EF-Tu (18). These large conformational changes between GTP- and GDP-bound EF-Tu have been suggested to induce the release of the tRNA from EF-Tu and the dissociation of EF-Tu from the ribosome (19). Recently, however, a crystal structure of EF-Tu with a nonhydrolyzable GTP analog (GDPNP) has been resolved in an open conformation, which together with single-molecule Förster resonance energy transfer (smFRET) experiments suggests that, when free in solution, GTP-bound EF-Tu samples a wide range of conformations (20). These results challenge the model that the identity of the nucleotide, GTP or GDP, acts as a switch for the conformations of EF-Tu. Further, smFRET experiments using dyes attached to different locations on EF-Tu suggest that GTP hydrolysis results in a smaller conformational change of ribosome-bound EF-Tu that is not compatible with the full transition to the open conformation (21). In the GTPase-activated conformation of ribosome-bound EF-Tu, before GTP hydrolysis, the γ-phosphate of GTP interacts with EF-Tu via the P-loop (V20, D21), the switch 1 loop (T61), and the switch 2 loop (G83) (3,17,22). The switch 1 loop in turn is involved in the binding of EF-Tu to the tRNA (nucleotides 1–3 and 73–75). The conformation of EF-Tu after GTP hydrolysis and $P_i$ release and before dissociation in the absence of antibiotics has not been structurally resolved yet.

Kirromycin (KIR) is an antibiotic that directly binds to the interface of EF-Tu domains D1 and D3 and prevents dissociation of EF-Tu from the ribosome and from the aa-tRNA after GTP hydrolysis (19,23–26). Structures of ribosome-bound EF-Tu with GDP and KIR have been obtained by x-ray crystallography and cryogenic electron microscopy (cryo-EM) (19,26). With KIR bound, the overall conformation of EF-Tu remains close to the GTP-bound conformation after hydrolysis, both on and off the ribosome (19,24–31). However, there seems to be a conformational difference between ribosome-bound EF-Tu in complex with GTP and with GDP plus KIR. In the ribosome-bound structures of either wild-type EF-Tu with nonhydrolyzable GTP analogs (3,17,22) or of a hydrolysis-incompetent EF-Tu variant (H84A) with GTP (17), the switch 1 loop is in the α-conformation. In the high-resolution structures with KIR+GDP (19,25,26), however, the switch 1 loop is not resolved, suggesting that it is more flexible in this state.

To resolve these experimental discrepancies and to elucidate how the antibiotic KIR prevents both dissociation of the tRNA from the ternary complex and release of the complex from the ribosome, we have carried out atomistic simulations of the full ribosome in explicit solvent. We investigated the conformational changes of the ternary complex after GTP hydrolysis and $P_i$ release while bound to the ribosome in the absence of KIR. Further, we addressed the

Please cite this article in press as: Warias et al., tRNA Dissociation from EF-Tu after GTP Hydrolysis: Primary Steps and Antibiotic Inhibition, Biophysical Journal (2019), https://doi.org/10.1016/j.bpj.2019.10.028



question of how these changes might lead to dissociation of the tRNA from EF-Tu and how they are prevented by KIR. To that aim, we used all-atom explicit-solvent molecular dynamics (MD) simulations started from cryo-EM structures of ribosome-bound *Escherichia coli* EF-Tu in complex with Phe-tRNA$^{Phe}$ and with either nonhydrolyzable GTP (3), with GDP and KIR (26), or with GDP after the removal of KIR. With bound GDP, in the absence of KIR, we found intermediate conformations of EF-Tu resulting in a weakened interaction between EF-Tu and the amino acid attached to the tRNA, suggesting that this intermediate prepresents a primary step toward the dissociation of the tRNA from EF-Tu and its accommodation into the A site.

## METHODS

### Ribosome complex MD simulations

To investigate the conformational changes of the ribosome-EF-Tu complex and the effect of GTP hydrolysis as well as of KIR, we carried out all-atom explicit-solvent MD simulations with GTP and with GDP and KIR as well as with GDP in the absence of KIR. As a starting structure for the simulations with GTP, the cryo-EM structure of an *E. coli* ribosome in complex with tRNAs, EF-Tu, and GTP was used (3) (protein data bank, PDB: 5UYM). For the simulations with GDP and KIR, the cryo-EM structures of an *E. coli* ribosome in complex with tRNAs, EF-Tu, GDP, and KIR were used (26) (PDB: 5AFI). For the simulations without KIR, KIR was removed from this starting structure. Protein L1 in the GTP and GDP structures and nucleotides of H38 in the GDP structure were not resolved and added to our model as described previously (32). In the GDP structure, residues 41–62 of EF-Tu were not resolved (26). To model these residues, a homology model EF-Tu was built using SWISS-MODEL (33) with the sequence of *E. coli* EF-Tu and GTP-bound x-ray structure of *Thermus aquaticus* EF-Tu (34) (PDB: 1EFT) as a structural template. After rigid-body fitting of residues 24–40 and 63–71 of the homology model to the corresponding residues in the cryo-EM structure, residues 41–62 of the homology model were included in our model.

All simulations were carried out using the GROMACS software package version 5.1 (35) with the amber99sb force field (36) and the SPC/E water model (37). Parameters from Joung and Cheatham (38) and from Aduri et al. (39) were used for $K^+Cl^-$ ions and modified nucleotides, respectively. Initial coordinates of KIR were extracted from the cryo-EM structure (26) and then protonated and energy minimized by a HF/6-31G* optimization in GAUSSIAN 09 (40). The electrostatic potential, calculated from the optimized structure at more than 140,000 points of a molecular surface around the KIR, was fitted to partial charges placed at the atomic positions using the ESPGEN module in AMBER (41). Additional force field parameters for KIR were obtained using the ANTECHAMBER module in AMBER. The parameters were converted for use in GROMACS using ACPYPE (42). Long-range electrostatics were calculated using the particle mesh Ewald method with grid spacing of 0.12 nm and a cutoff of 1 nm (43). Van der Waals interactions were calculated for atoms within 1 nm of each other.

The complex was placed in a dodecahedron box with a minimum distance of 1.5 nm between box borders and any solute atom, and then, the box was solvated with water molecules. Next, the charge of the system was neutralized by adding $K^+$ ions using the GENION program from the GROMACS package. Then, $Mg^{2+}$ and $Cl^-$ ions with a concentration of 7 mM and $K^+Cl^-$ ions with a concentration of 150 mM were added.

For each case, GTP, GDP with KIR, and GDP without KIR, we ran two independent simulations. Each simulation system was equilibrated in four steps as described previously (32):

1) Energy minimization using steepest decent.
2) 0–50 ns: Position restraints on all atoms that were resolved in the cryo-EM structure (force constant $k = 1000$ kJ//mol/nm$^2$) and Berendsen barostat (44) ($\tau_p = 1$ ps).
3) 50–70 ns: Linear decrease of position restraint force constant $k$ to zero.
4) 70–2070 ns (70–1070 ns for GTP): No position restraints and Parrinello-Rahman barostat (45) ($\tau_p = 1$ ps).

In all simulations, the bond lengths were constrained using the LINCS algorithm (46). Virtual site constraints (47) and an integration step of 4 fs were used. The temperature of solute and solvent was controlled independently using velocity rescaling (48) ($\tau_T = 0.1$ ps). Production runs consisted of 1 and 2 $\mu$s of unrestrained MD simulations for GTP and GDP (with and without KIR), respectively. Only these trajectories, recorded every 5 ps, were used for analysis.

### MD simulations of EF-Tu in solution

To test whether the opened D1-D3 interface is energetically unfavorable, we performed simulations of EF-Tu in complex with aa-tRNA and GTP in solution started from a conformation with an open D1-D3 interface. The starting structure was taken from a GTPase-activated ribosome EF-Tu aa-tRNA structure (3). All ions resolved in the cryo-EM structure within a 15-Å radius around the tRNA and EF-Tu were kept for the simulation system. The setup then followed the same steps as the simulations of the ribosome complex (see above).

### Principal component analysis

To obtain the dominant conformational modes of motion for EF-Tu and the tRNA, we employed principal component analysis (PCA) (49). The eigenvectors of the covariance matrix were calculated using the program gmx covar from the GROMACS package (35). To identify the modes of EF-Tu's domain D1 relative to the other two domains, we first rigid-body fitted the nitrogen and both carbon atoms of the backbone of residues 210–294 and 303–393 for each frame of each trajectory to the corresponding atoms of the cryo-EM structure (26). The covariance matrix was then constructed from the concatenated trajectories of nitrogen and carbon atoms of the backbone of residues 11–198 (D1).

### Residue distances

To measure the opening of the domain interfaces of EF-Tu, which bind either the CCA tail of the tRNA or KIR, distances between EF-Tu residues as a function of simulation time were calculated from the trajectories. For the KIR binding site located between domains D1 and D3, the distance between the C$\alpha$ atoms of residues Q124 and E373 was calculated. The opening of the tRNA binding cleft was observed by measuring the distance between the C$\alpha$ atoms of residues H66 and E259. To measure the degree of tRNA accommodation, we measured the distance $R_{elbow}$, as defined previously (13), between the O3′ atoms of nucleotides U8 (P-site tRNA) and U60 (A-site tRNA) from the trajectories and cryo-EM structures (3,17).

### Volume overlap

To test whether the conformational motion of D1 relative to D2 and D3 observed in simulations without KIR can also occur in the presence of KIR, we investigated if this motion would lead to a clash between KIR and EF-Tu. To that aim, we first extracted snapshots at an interval of 4 ns from trajectories. These snapshots were then rigid-body fitted to the cryo-EM structure using coordinates of all atoms of D1 of EF-Tu. Next, the overlap of the Van der Waals volume from EF-Tu from the trajectory with that of the KIR from the cryo-EM structure was calculated. To calculate this overlap, we first calculated the Van der Waals volumes $V_{EF\text{-}Tu}$, $V_{KIR}$, and $V_{EF\text{-}}$

$_{Tu+KIR}$ for the EF-Tu atoms, for the KIR atoms, and for the combined set of atoms, respectively, using Monte Carlo integration. To this aim, all EF-Tu atoms within 1 nm of KIR were selected, and then, $20 \times 10^6$ points were randomly placed in a box defined by extensions of the atomic coordinates. The volume is then calculated by $V =$ (Number of points inside Van der Waals sphere)/(Total number of points) $\times$ (Box volume). The overlap $V_{overlap}$ is then gained by $V_{overlap} = V_{EF\text{-}Tu} + V_{KIR} - V_{EF\text{-}Tu+KIR}$.

## Free-energy calculation of D1-D3 interface closure

To estimate the free-energy difference between EF-Tu with an open and closed D1-D3 interface, we used umbrella sampling simulations (50) along a reaction coordinate representing the closing motion. To obtain the reaction coordinate, first, the trajectories of the ribosome-EF-Tu complexes were rigid-body fitted using D1 atoms to the cryo-EM structure, and, second, a PCA of the D3 atom coordinates was performed (atom selection as described in Principal component analysis). The first eigenvector obtained from the PCA was chosen as the reaction coordinate. The first simulation of the isolated ternary complex that showed a transition from the open to the closed conformation (sim5) was projected onto this reaction coordinate. Then, 51 equally spaced projections were chosen as windows for the umbrella sampling. For each window, first, a structure corresponding to the projection values was extracted. Next, from each of these structures, a 75-ns MD simulation was started with an additional umbrella potential centered at the corresponding projection value and a spring constant of 100 kJ/mol/nm$^2$. The first 10 ns of each trajectory were discarded to allow for equilibration. Free energies were calculated using the g_wham tool, and the errors were estimated by 300 bootstrapping steps (51).

## Interaction enthalpies

To estimate whether the conformational motion of EF-Tu, observed in the simulations, changes the binding strength between EF-Tu and the aa-tRNA, we calculated interaction enthalpies between the tRNA (nucleotide A76 and attached amino acid F77) and EF-Tu domains D1 and D2. Interaction enthalpies were calculated every 5 ps using the rerun option of the GROMACS package. To check if the opening of the D1-D2 interface weakens these interactions, for domain and each simulation of ribosome-bound EF-Tu, the correlation coefficient of the H66–E259 distance and the interaction enthalpy was calculated. Subsequently, for each domain, mean and SDs for these correlation coefficients were calculated.

## 30S head and body rotation

To monitor the conformational changes of the ribosome during the simulations, the 30S body rotation and 30S head swivel angles were calculated from the trajectories and cryo-EM structure (3,26), as described previously (52) using the MDAnalysis toolkit (53).

# RESULTS AND DISCUSSION

After GTP hydrolysis and $P_i$ release, EF-Tu changes its conformation, ultimately resulting in tRNA accommodation and EF-Tu release. To investigate the conformational changes of EF-Tu after $P_i$ release, we performed MD simulations of the ternary complexes EF-Tu-GTP-aa-tRNA and EF-Tu-GDP-aa-tRNA bound to the ribosome, started from cryo-EM structures (3,26). For the GDP-bound conformation, the unresolved switch 1 loop was modeled based off its GTP-bound conformation (34), and two simulations, including KIR and two simulations after the removal of KIR, were carried out for 2 $\mu$s each. As a control, two 1-$\mu$s simulations with GTP were carried out.

## Dynamics of switch 1 loop after $P_i$ release

In the GTP-bound conformation, switch 1, switch 2, and P-loop residues of EF-Tu are in contact with GTP (3,17,22). The only direct contact of the switch 1 loop with GTP is between Thr61 and the $\gamma$-phosphate (Fig. 1 *c*; (3,22)). This contact is lost after hydrolysis and $P_i$ release. To test if the loss of this specific contact results in either different contacts or in a complete loss of contacts between the switch 1 region and the nucleotide, we monitored the contact occupancies of the $\beta$-phosphate with the P-loop and switch 1 region over the course of our simulations (Fig. 2 *a*). Here, the criterion for a contact between a residue and the $\beta$-phosphate was that any nonhydrogen atom of the residue was within 5 Å of the $\beta$-phosphate. The contacts with the P-loop that were present in the GTPase-activated state (3,22) (residues 19–24) remained present in all the simulations. As expected, the contact between GTP and Thr61 of the switch 1 loop was stable in the simulations with GTP-bound EF-Tu. In contrast, in all simulations of GDP-bound EF-Tu, we observed a rapid loss of the contact between GDP and Thr61. In one of the simulations, which included GDP and KIR (sim1), we observed spurious occurrences of contacts between the $\beta$-phosphate and residues 59 and 60, which are not present in the GTP-bound conformation (3,22). The loss of contacts between switch 1 and GDP suggests that it is the presence of the $\gamma$-phosphate that keeps the switch 1 region in place. This result is consistent with the structures of EF-Tu-KIR-GDP-aa-tRNA bound to the ribosome, in which GDP is bound to P-loop and the switch 1 region is not resolved (19,25,26). The observation that the switch 1 region is not resolved in these structures indicates that the region is more flexible than the rest of EF-Tu. To check if the loss of contacts between GDP and switch 1 results in an increased flexibility of the switch 1 region, we calculated the root mean-square fluctuation of the backbone atoms in all domains of EF-Tu (Fig. 2 *b*). Indeed, when GDP is bound, the switch 1 region is markedly more flexible than with GTP bound. The switch 1 loop is also more flexible compared to the P-loop and the switch 2 region. The residues with large flexibility correspond well with the unresolved residues in KIR-bound structures (19,26) (Fig. 2 *b*, *black horizontal bars*). In one simulation with bound KIR (sim2), the switch 1 loop is more flexible than in the other (sim1). Differences are expected because the timescales of the simulations do not allow the flexible loop to explore all conformations. However, for both simulations, the overall conformation of EF-Tu, excluding the switch 1 loop, is very similar to the cryo-EM structure (26), implying that this difference is probably not important for the mechanism.

Please cite this article in press as: Warias et al., tRNA Dissociation from EF-Tu after GTP Hydrolysis: Primary Steps and Antibiotic Inhibition, Biophysical Journal (2019), https://doi.org/10.1016/j.bpj.2019.10.028



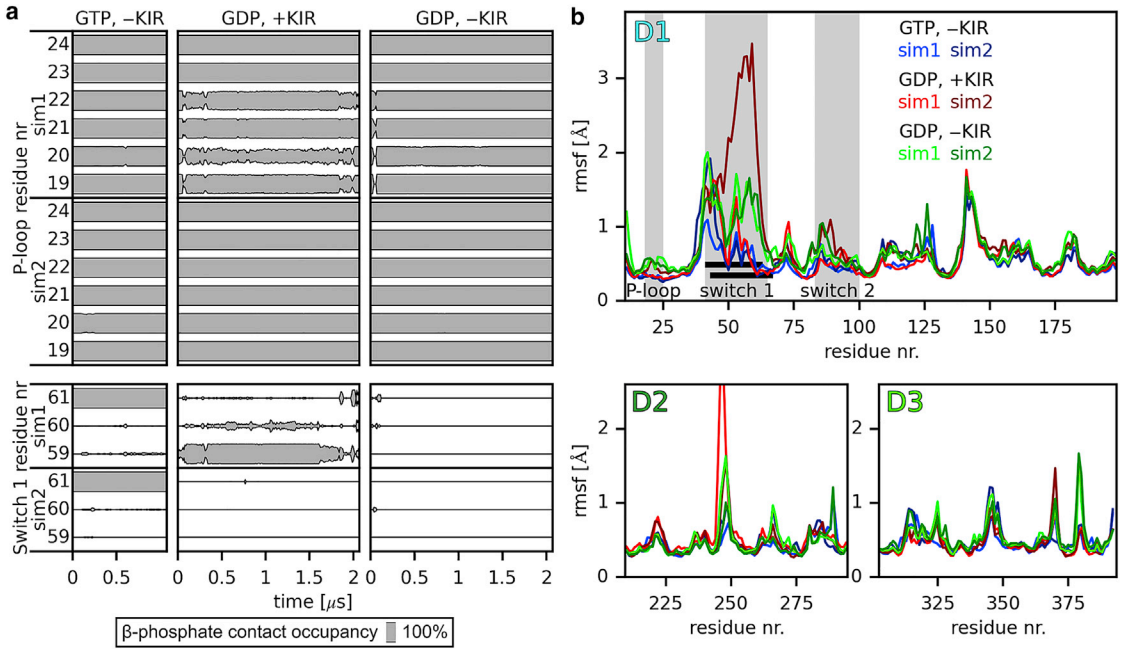


FIGURE 2 (*a*) Contacts of EF-Tu residues with the $\beta$-phosphate of GTP or GDP. For residues of the P-loop of EF-Tu (*upper panel*) and the switch 1 loop (*lower panel*), the occupancy of contacts with the $\beta$-phosphate (distance below 5 Å) was monitored over the course of the simulations (sim1 and sim2) with GTP and with GDP in the presence and absence of KIR (*columns*). (*b*) Atomic fluctuations of EF-Tu. For each domain of EF-Tu, D1, D2, and D3, the root mean-square fluctuation (rmsf) for each residue is shown for each simulation. The P-loop, switch 1, and switch 2 regions of domain D1 are highlighted in gray. Black bars denote the residues that are unresolved in structures of ribosome-bound EF-Tu in complex with GDP and KIR (19,26).

These results suggest that after $P_i$ release, the switch 1 region is not anchored to the rest of domain D1 anymore and can explore a larger range of conformations.

## Interdomain motions of EF-Tu

To elucidate the consequences of the GDP-induced higher switch 1 flexibility on the EF-Tu conformation, we first investigated the interdomain motions of EF-Tu. The two interfaces between domains D1 and D2 and between D1 and D3 are functionally important. The D1-D2 interface is where the CCA tail of the tRNA along with the attached amino acid are bound. The observation that deacylated tRNAs have a lower affinity to EF-Tu underscores the importance of this interaction for a stable ternary complex (54,55). Further, antibiotics that bind to the D1-D2 interface prevent the binding of a tRNA to EF-Tu and therefore the formation of the ternary complex (56). The D1-D3 interface is the binding site of the antibiotic KIR, which hinders the release of the tRNA from EF-Tu. Notably, the D1-D3 interface is observed to be closed in x-ray structures of the isolated ternary complex with a distance of 6.5 Å between the C$\alpha$ atoms of residues Q124 (D1) and R373 (D3) (15). The interface remains closed when EF-Tu binds to the ribosome in the initial binding and the codon recognition states with distances of 5.3 and 5.1 Å, respectively (3). Upon GTPase activation, the interface opens (9.5 Å (3)), even more so when KIR is bound (11.6 Å (26)). The D1-D2 interface remains closed around the CCA tail of the tRNA in all of these steps.

EF-Tu domains D2 and D3 stay in a very similar conformation relative to each other, both in all the structures and during all the simulations. To investigate the motion of EF-Tu after hydrolysis and $P_i$ release, we used PCA to extract the dominant conformational modes of the motion of D1 relative to D2 and D3 (49). Fig. 3 *a* shows the reaction coordinates of the D1 motion (i.e., the projections onto the dominant mode) as well as the distances between EF-Tu residues H66–E259 and Q124–R373, which report on the closing or opening of the D1-D2 and D1-D3 interfaces, respectively. This D1 reaction coordinate describes a rotation of D1 around the switch 2 helix. To indicate which conformations are observed in the simulations, the logarithm of the probability densities obtained from the simulations are shown for the ribosome-bound ternary complex with either GTP or GDP (with and without KIR) as well as for the isolated ternary complex (with GTP, lower panel). For sufficient sampling, this quantity would represent the free-energy landscape that governs the conformational dynamics in units of $k_bT$. The most probable conformations for each case of ribosome-bound EF-Tu are shown in Fig. 3 *b*, and their positions are indicated with circles in Fig. 3 *a*. In the simulations with GTP as well as with GDP and KIR, EF-Tu remains close to the respective starting structures (GA and KIR in Fig. 3 *a*) with open D1-D3 and closed D1-D2 interfaces, which is expected and therefore supports the

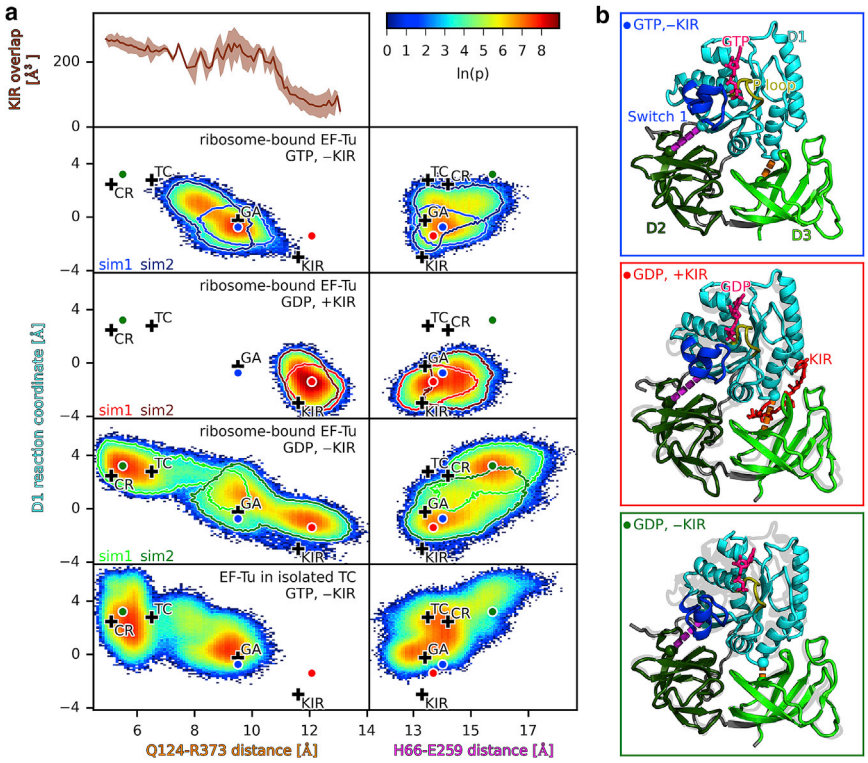


FIGURE 3 Conformational dynamics of ribosome-bound EF-Tu with GTP, GDP (with and without KIR), and EF-Tu in the isolated ternary complex with GTP. (*a*) The trajectories of the MD simulations were projected onto the reaction coordinates of the D1 motion and the C$\alpha$ distances between residues Q123 and R373 as well as H66 and E259. The color represents the logarithm of the probability density $\rho$. Black crosses correspond to the positions of available structures of EF-Tu: in the ternary complex with GTP (TC (15)), bound to the ribosome in the codon-reading (CR (3)) and GTPase-activated (GA (3)) states, and in the KIR-bound state with GDP (KIR (26)). Circles indicate the largest probability densities obtained for the complex with GTP (*blue*), with GDP and with KIR (*red*), and with GDP and without KIR (*green*). For simulations of ribosome-bound EF-Tu, the outlines correspond to $\ln(p) = 2$ for simulations sim1 and sim2. KIR overlap as a function of Q124–R373 distance, which denotes the van der Waals overlap between the KIR atoms and EF-Tu atoms after rigid-body fitting KIR into all trajectories of ribosome-bound EF-Tu. (*b*) The conformations corresponding to the largest probability densities (*colored circles*) are depicted. D1, D2, and D3 are colored in cyan, dark green, and light green, respectively. Switch 1 loop and P-loop of EF-Tu are colored in blue and yellow, respectively, as well as GTP and GDP in pink.

validity of the starting structure and the simulation setup. In the simulations with GDP and without KIR, started from the KIR-bound cryo-EM structure, the D1-D3 interface closed fully, reaching the codon-reading state in one of the simulations (Fig. 3 *a*, sim1, *light green outline*) and closed partially, reaching the GA state in the other (sim2, *dark green outline*). In the case of full interface closure, the Q124–R373 distance dropped rapidly during the first 200 ns from the initial 12 Å observed in the KIR-bound cryo-EM structure to around 6 Å, and the interface remains closed for the rest of the simulation. This distance is close to the distances observed in the isolated ternary complex as well as the initial binding and codon recognition states (3,15). In the case of partial closure, after an initial drop to around 9 Å, the distance returns to around 12 Å. The Q124–R373 distance correlates strongly with the D1 reaction coordinate. Notably, the motion of D1 also correlates with an opening of the D1-D2 interface as can be seen by an increase in the H66–E259 distance to around 16 Å. This extent of D1-D2 interface opening is not seen in structures of EF-Tu with either GTP or with GDP-KIR, in which the H66–E259 distance ranges only from 13.3 to 14.2 Å (3,15,26).

To investigate if the presence of KIR in the D1-D3 interface sterically prevents the closing, we calculated the Van der Waals overlap between KIR atoms and EF-Tu atoms after rigid-body fitting KIR into the binding site of structures obtained from the simulations with and without KIR. Fig. 3 *a* shows that this overlap increases with decreasing Q124–R373 distances, indicating that KIR indeed acts as a steric block, preventing the closure of the D1-D3 interface and thereby the opening of the D1-D2 interface.

In summary, these results suggest that upon GTP hydrolysis, $P_i$ release results in a loss of the switch 1 loop anchoring to the rest of D1, which frees D1 to rotate around the switch 2 helix. This rotation closes the D1-D3 interface and opens the D2-D3 interface, possibly decreasing the interaction of EF-Tu with the amino acid and the CCA tail of the tRNA and, therefore, the affinity of the tRNA to EF-Tu. The presence of KIR interrupts this sequence of events; it thus does not interfere with GTP hydrolysis and $P_i$ release but sterically hinders the closing of the D1-D3 interface, which in turn prevents the rotation of D1 and the opening of the D1-D2 interface.

## Effect of the ribosome on the D1-D3 interface conformation

The D1-D3 interface of ribosome-bound EF-Tu is in an open conformation in the GTPase-activated state and even further opened in the KIR-stalled state (Fig. 3 *a*). In all other structures of the ternary complex, whether bound to the ribosome or free, the D1-D3 interface is closed. The spontaneous closure of this interface, observed in our simulations, raises the question of if the closed conformation is intrinsically favorable for EF-Tu, and the open conformation is induced by interactions with the tRNA and ribosome in the GTPase-activated state. If this were the case, the open

Please cite this article in press as: Warias et al., tRNA Dissociation from EF-Tu after GTP Hydrolysis: Primary Steps and Antibiotic Inhibition, Biophysical Journal (2019), https://doi.org/10.1016/j.bpj.2019.10.028



interface conformation could resemble the loaded spring, which is released only upon GTP hydrolysis and subsequent $P_i$ release, as suggested earlier (6). To test if this is actually the case, we performed six additional simulations of the free ternary complex in solution started from the open GTPase-activated conformation (3).

Fig. 3 *a* (*lower panel*) shows the H66–E259 and Q124–R373 distances relative to the D1 motion for these simulations. In five out of the six simulations, the Q124–R373 distance decreased to around 6 Å, thereby closing the D1-D3 interface after simulation times ranging from less than 10 ns to 1 $\mu$s (Fig. 4 *a*). The fact that EF-Tu transitions to a closed conformation in all but one of the simulations—without back transitions—implies that the closed conformation is indeed energetically favorable in the absence of the ribosome. To further test this conclusion, we calculated the free-energy landscape of the interface closure by additional umbrella sampling simulations. Fig. 4 *b* shows the resulting free-energy landscape as a function of the D1-D3 domain closing motion (D3 reaction coordinate, see Methods). Clearly, the closed state is energetically more favorable, which combined with the spontaneous closing in the GDP-bound simulations, further corroborates the idea that the D1-D3 interface opens in the GTPase-activated state by interaction with the ribosome.

Whereas the D1-D3 interface closed in almost all GTP-bound ternary complex simulations, the D1-D2 interface remained closed (Fig. 3 *a*). This result, together with the increased flexibility of the switch 1 loop observed in GDP-bound simulations of EF-Tu in the ribosome, provides additional support to the idea that the interaction between the switch 1 loop and the $\gamma$-phosphate stabilizes the D1-D2 interface in the closed conformation.

## Change of interactions between EF-Tu and aa-tRNA

For the tRNA to fully accommodate into the ribosomal A site, it has to dissociate from EF-Tu. The CCA tail of the tRNA (nucleotides 74–76) and the attached amino acid (F77) are sandwiched between EF-Tu domains D1 and D2, in which A76 and F77 are in contact with E259 and H66 of EF-Tu, respectively (3,15,26). The opening of the D1-D2 interface observed in the simulations of ribosome-bound EF-Tu after the hydrolysis and removal of KIR suggests that this conformational change may weaken the interaction between EF-Tu and the aa-tRNA. To test this possibility, we calculated the interaction enthalpies of A76 and F77 with all D1 and with all D2 residues (Fig. 5). The enthalpy of the interactions with the D2 domain is not correlated with the H66–E259 distance opening of the D1-D2 interface (correlation coefficient 0.09 $\pm$ 0.07). In contrast, the interactions with the D1 domain are weakened (less negative interaction enthalpies) with increased H66–E259 distance (Fig. 5 *a*, correlation coefficient 0.35 $\pm$ 0.09). Closer analysis of the obtained trajectories revealed that when the D1-D2 interface opened, A76 of the tRNA and the backbone of F77 remained bound to domain D2, whereas F77 tilted away from D2, maintaining weak interactions with D1 (Fig. 5). This conformational change results in an overall weakening of F77 interactions with EF-Tu, which we therefore suggest as the primary step of the tRNA 3′ end dissociation from EF-Tu.

After dissociation from EF-Tu, the tRNA accommodates into the A site (1). During the first accommodation step, the accommodation of the tRNA elbow, the distance between the elbow regions of the A site and P site tRNAs ($R_{elbow}$) decreases from ~50 to ~30 Å (12). As expected from the observation that EF-Tu is not fully dissociated from the tRNA in the simulations, the elbow distance remains close to its values in the cryo-EM structures used as starting structures for the simulations (Fig. 5 *c*). In the GTPase-activated and KIR-blocked cryo-EM structures, the body of 30S subunit relative to the 50S subunit is rotated by only ~1° (GA, KIR in Fig. 5 *d*) when compared to the classical conformation (0°, (57)). The 30S head is swiveled by about −1° compared to the classical conformation (Fig. 5 *e*). During the simulations, we observed spontaneous head and body rotations around these values in a range expected from previous MD simulations (52,58,59). These results suggest that the conformational changes of EF-Tu and the primary steps of its dissociation do not lead to tRNA

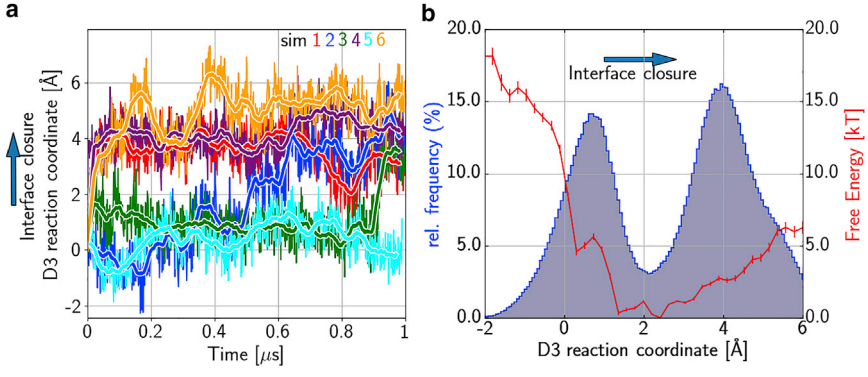


FIGURE 4 Spontaneous D1-D3 interface closure of EF-Tu in the isolated ternary complex. (*a*) For six unrestrained MD simulations, started from a conformation with an open interface, the projection onto the D3 reaction coordinate describing the interface closure is shown as a function of simulation time (*colored lines*; *thick lines*: running averages). (*b*) Potential of mean force (PMF, *red line*) as a function of the reaction coordinate. Error bars were estimated by bootstrapping. The histogram of the concatenated projections of the six unrestrained MD simulations is shown (*blue line*).

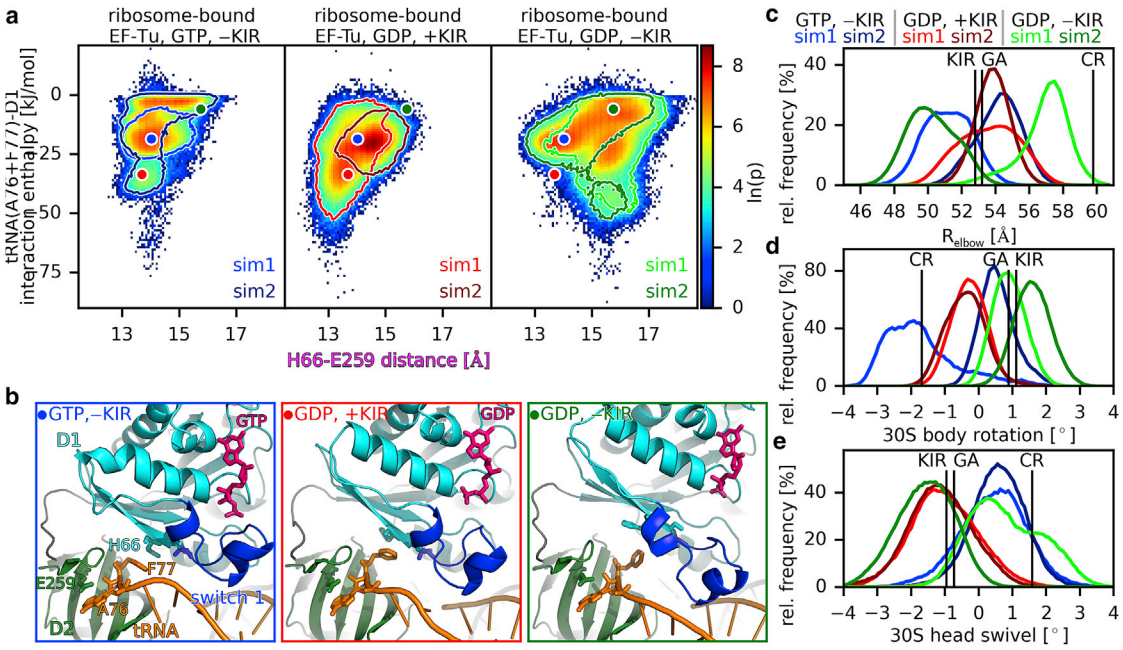


FIGURE 5 EF-Tu-tRNA interactions, tRNA movement, and inter-subunit rotation. (*a*) The probability density $\rho$ as a function of the H66–E259 distance (D1-D2 opening) and of the interaction enthalpy of nucleotide A76 (tRNA) and amino acid F77 (attached to the tRNA) with EF-Tu domain D1 is shown for the simulations of ribosome-bound EF-Tu. The circles denote the positions of the conformations shown in Fig. 3. (*b*) Close up on the D1-D2 interface for these conformations with colors as in Fig. 3 *b* and the tRNA in orange. (*c*) Histograms of the distance between the elbows of the EF-Tu-bound tRNA and of the P-site tRNA were obtained from the different simulations (*colors*). (*d* and *e*) Histograms of 30S body rotation angles and 30S head swivel angles relative to the classical state (57).

accommodation or large-scale conformational changes of the ribosomes in the timescales of the simulations.

## CONCLUSIONS

Successful decoding of the messenger RNA codon in the ribosomal A site by the ternary complex EF-Tu-GTP-tRNA results in a GTPase-activated conformation of EF-Tu (3–5). After GTP hydrolysis and the release of the inorganic phosphate $P_i$, the ribosome-bound EF-Tu undergoes a conformational change that precedes the release of EF-Tu from the ribosome (6,21). This conformational change ultimately results in the release of the tRNA from EF-Tu, allowing the tRNA to fully accommodate into the A site and EF-Tu to dissociate from the ribosome. Here, using MD simulations started from cryo-EM structures of the ribosome in complex with EF-Tu-tRNA-GTP (3) and EF-Tu-tRNA-GDP, which has been stalled by KIR (26), we have investigated the primary conformational changes and energetics of EF-Tu after hydrolysis and how they might lead to tRNA release.

In structures of ribosome-EF-Tu complexes with inhibited GTP hydrolysis, the switch 1 loop of domain D1 of EF-Tu is resolved and interacts with the tRNA and the $\gamma$-phosphate of GTP (3,17). In our simulations of the state after hydrolysis and $P_i$ release, we observed a loss of the contacts between the switch 1 loop and GDP (Fig. 6). GDP remained firmly bound to the rest of the D1 domain, whereas the switch 1 loop interacted with the tRNA throughout the simulations and was markedly more flexible than most other parts of EF-Tu. This observation is consistent with previous MD simulations of the isolated domain D1 started from the GTP-bound conformation, in which the switch 1 loop in simulations with GDP was more flexible than with GDP (60), supporting the notion that the $\gamma$-phosphate interactions stabilize the switch 1 loop. This result can explain why in cryo-EM structures of the ribosome-EF-Tu complex, in which the dissociation after GTP hydrolysis is prevented by the antibiotic KIR, switch 1 loop is not resolved (19,25,26). Vice versa, the fact that the same part that shows high flexibility in our simulations is not resolved in the structures provides independent support for our simulations. After the loss of the interactions between the switch 1 loop and the rest of D1, which, before hydrolysis, were stabilized by the $\gamma$-phosphate, D1 is free to rotate toward D3. This rotation results in the closing of the D1-D3 and opening of the D1-D2 interface, within which the CCA tail of the tRNA and its attached amino acid are bound. We therefore propose that before hydrolysis, the switch 1 loop anchors domain D1 to D2 via the interaction with the $\gamma$-phosphate. In our simulations, the opening of the D1-D2 interface reduced the interaction between EF-Tu and the amino acid attached to the tRNA, whereas the tRNA interactions with D3 remain. This result agrees with and explains in structural terms previous ensemble kinetics experiments, which indicated that the 3′ end of the tRNA dissociates from EF-Tu first, preceding the full dissociation (8).

Please cite this article in press as: Warias et al., tRNA Dissociation from EF-Tu after GTP Hydrolysis: Primary Steps and Antibiotic Inhibition, Biophysical Journal (2019), https://doi.org/10.1016/j.bpj.2019.10.028



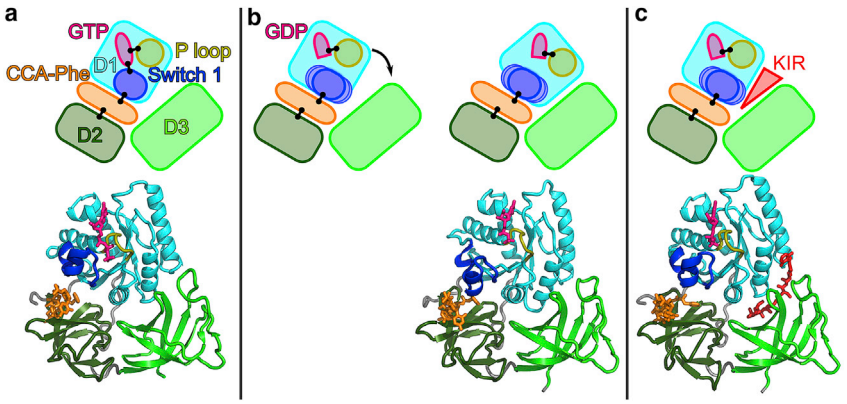


FIGURE 6 Proposed primary step of EF-Tu after GTP hydrolysis and the mechanism of KIR. (*a*) The conformation of the ribosome-bound EF-TU in the GTPase-activated state. Upper panel: Sketch of the domains of EF-Tu (D1, D2, and D3 in *cyan*, *dark green*, and *light green*), specific parts of D1 (switch 1 loop and P-loop, in *blue* and *yellow*, respectively), and the tRNA CCA tail with attached Phe (*orange*), GTP (*pink*), and KIR (*red*). Contacts discussed in the text are represented by black lines. Lower panel: structure of the GTPase-activated state of EF-Tu (3). (*b*) After hydrolysis to GDP (*pink*) and $P_i$ release (not shown), the contact between GDP and the switch 1 loop is lost, and the switch 1 loop becomes flexible. Because D1 is not restrained by the contact to switch 1, it rotates (*black arrow*) toward D3 into an energetically favorable conformation, thereby opening the D1-D2 and closing the D1-D3 interface. The structure of the last frame of the MD simulation in the absence of KIR (sim1) is shown. (*c*) KIR bound to the D1-D3 interface sterically blocks the D1 rotation. The structure of KIR-stalled EF-Tu is shown (26).

The weakening of interaction enthalpies between F77 and EF-Tu upon D1-D2 interface opening was observed between F77 and D2 residues and, to a lesser degree, between F77 and D1 residues. The interaction between F77 and D1 was mainly with histidine 66, which strongly contributes to the affinity of Phe-$tRNA^{Phe}$ to EF-Tu and, to a lesser degree (or not at all), to that of other tRNAs (61). This specificity of the interaction between the attached amino acid and EF-Tu suggests that the details of dissociation of the 3′ end of the tRNA most likely depend on the amino acid. Nevertheless, we would expect the opening of the D1-D2 interface to destabilize the interaction between EF-Tu and all other amino acids as well.

Because of the relatively short timescales that can currently be covered with unrestrained explicit-solvent all-atom MD simulation (62), the subsequent steps of full EF-Tu dissociation from the ribosome and the tRNA are not observed in our simulations. Based on biased MD simulations, Lai et al. proposed a pathway from the closed GTP-bound conformation to the open GDP-bound conformation, which involves a separation of D1 from D2 and D3, followed by a rotation of D1 and a subsequent rejoining of D1 with D2 and D3 in the GTP-bound conformation (63). Unrestrained coarse-grained MD simulations of the transition of EF-Tu between the GTP- and the GDP-bound conformation suggested that multiple routes exist, including a direct path, paths involving domain separation, and more disordered intermediate conformations (64). A combination with coarse-grained simulations of tRNA accommodation (65) suggested that these disordered conformations affect the kinetics of tRNA accommodation (64). In agreement with our observations, no spontaneous transitions were observed in unbiased all-atom MD simulations on a $\mu$s timescale (63,64).

Interestingly, the D1-D3 interface is closed in all structures of the isolated GTP-bound ternary complex and in ribosome-bound conformations, except for the GTPase-activated structure (3). This observation indicates that the EF-Tu conformation with an open D1-D3 interface is stabilized by interactions with the ribosome in the GTPase-activated state. It also suggests that upon GTP hydrolysis, D1 is able to rotate and reverts back into the energetically preferred closed D1-D3 conformation.

The antibiotic KIR binds to the D1-D3 interface and thereby sterically hinders the D1 rotation. As a result, the D1-D2 interface remains closed around the 3′ end of the tRNA in our simulations, including KIR, maintaining strong interactions with the 3′ end, thereby preventing the dissociation of the 3′ end from EF-Tu. We propose that the prevention of this first dissociation step prevents full EF-Tu dissociating from the tRNA and the ribosome after GTP hydrolysis and thus locks EF-Tu into a conformation close to the prehydrolysis conformation (23,24).

Several other antibiotics are similar to KIR in structure and binding site, and therefore, the proposed mechanism may apply to a larger class of antibiotics (66–69). For example, aurodox has been shown to occupy the same binding site in the same conformation as KIR (69). Further, this structure contains GDP, and the switch 1 loop is not fully resolved, indicating that aurodox stalls EF-Tu on the ribosome in the same way as KIR. But also structurally unrelated antibiotics, such as enacyloxin IIa, bind to the D1-D3 interface in a binding site, which overlaps with that of KIR (70,71), result in an open D1-D3 interface, and prevent the dissociation of EF-Tu-GDP from the ribosome. The observation that a differently structured antibiotic, which occupies the same binding site as KIR, has the same effect, is further experimental support for the idea that KIR sterically hinders the domain closure, which appears to be a necessary primary step of EF-Tu release from the tRNA and the ribosome, and suggests a general mechanism.

## AUTHOR CONTRIBUTIONS

L.V.B. and M.W. performed the MD simulations of the ribosome-bound and the free ternary complex, respectively. M.W. and L.V.B. analyzed the data. All authors discussed the results and wrote the manuscript.

Please cite this article in press as: Warias et al., tRNA Dissociation from EF-Tu after GTP Hydrolysis: Primary Steps and Antibiotic Inhibition, Biophysical Journal (2019), https://doi.org/10.1016/j.bpj.2019.10.028



## ACKNOWLEDGMENTS

This research was supported by the Deutsche Forschungsgemeinschaft Forschergruppe FOR1805 (to H.G. and L.V.B.). We thank the Max Planck Computing and Data Facility (MPCDF) and the Gesellschaft für wissenschaftliche Datenverarbeitung Göttingen for technical assistance; computer time has been provided by the MPCDF.

## REFERENCES

1. Rodnina, M. V., N. Fischer, …, H. Stark. 2017. Ribosome dynamics during decoding. *Philos. Trans. R Soc. Lond. B Biol. Sci.* 372:20160182.
2. Ogle, J. M., F. V. Murphy, IV, …, V. Ramakrishnan. 2002. Selection of tRNA by the ribosome requires a transition from an open to a closed form. *Cell.* 111:721–732.
3. Loveland, A. B., G. Demo, …, A. A. Korostelev. 2017. Ensemble cryo-EM elucidates the mechanism of translation fidelity. *Nature.* 546:113–117.
4. Adamczyk, A. J., and A. Warshel. 2011. Converting structural information into an allosteric-energy-based picture for elongation factor Tu activation by the ribosome. *Proc. Natl. Acad. Sci. USA.* 108:9827–9832.
5. Mondal, D., and A. Warshel. 2018. EF-Tu and EF-G are activated by allosteric effects. *Proc. Natl. Acad. Sci. USA.* 115:3386–3391.
6. Kothe, U., and M. V. Rodnina. 2006. Delayed release of inorganic phosphate from elongation factor Tu following GTP hydrolysis on the ribosome. *Biochemistry.* 45:12767–12774.
7. Pape, T., W. Wintermeyer, and M. V. Rodnina. 1998. Complete kinetic mechanism of elongation factor Tu-dependent binding of aminoacyl-tRNA to the A site of the *E. coli* ribosome. *EMBO J.* 17:7490–7497.
8. Liu, W., C. Chen, …, B. S. Cooperman. 2015. EF-Tu dynamics during pre-translocation complex formation: EF-Tu·GDP exits the ribosome via two different pathways. *Nucleic Acids Res.* 43:9519–9528.
9. Geggier, P., R. Dave, …, S. C. Blanchard. 2010. Conformational sampling of aminoacyl-tRNA during selection on the bacterial ribosome. *J. Mol. Biol.* 399:576–595.
10. Polikanov, Y. S., A. L. Starosta, …, D. N. Wilson. 2015. Distinct tRNA accommodation intermediates observed on the ribosome with the antibiotics hygromycin A and A201A. *Mol. Cell.* 58:832–844.
11. Sanbonmatsu, K. Y., S. Joseph, and C. S. Tung. 2005. Simulating movement of tRNA into the ribosome during decoding. *Proc. Natl. Acad. Sci. USA.* 102:15854–15859.
12. Whitford, P. C., P. Geggier, …, K. Y. Sanbonmatsu. 2010. Accommodation of aminoacyl-tRNA into the ribosome involves reversible excursions along multiple pathways. *RNA.* 16:1196–1204.
13. Noel, J. K., and P. C. Whitford. 2016. How EF-Tu can contribute to efficient proofreading of aa-tRNA by the ribosome. *Nat. Commun.* 7:13314.
14. Berchtold, H., L. Reshetnikova, …, R. Hilgenfeld. 1993. Crystal structure of active elongation factor Tu reveals major domain rearrangements. *Nature.* 365:126–132.
15. Nissen, P., M. Kjeldgaard, …, J. Nyborg. 1995. Crystal structure of the ternary complex of Phe-tRNAPhe, EF-Tu, and a GTP analog. *Science.* 270:1464–1472.
16. Kjeldgaard, M., and J. Nyborg. 1992. Refined structure of elongation factor EF-Tu from *Escherichia coli*. *J. Mol. Biol.* 223:721–742.
17. Fislage, M., J. Zhang, …, J. Frank. 2018. Cryo-EM shows stages of initial codon selection on the ribosome by aa-tRNA in ternary complex with GTP and the GTPase-deficient EF-TuH84A. *Nucleic Acids Res.* 46:5861–5874.
18. Abel, K., M. D. Yoder, …, F. Jurnak. 1996. An $\alpha$ to $\beta$ conformational switch in EF-Tu. *Structure.* 4:1153–1159.
19. Schmeing, T. M., R. M. Voorhees, …, V. Ramakrishnan. 2009. The crystal structure of the ribosome bound to EF-Tu and aminoacyl-tRNA. *Science.* 326:688–694.
20. Johansen, J. S., D. Kavaliauskas, …, C. R. Knudsen. 2018. *E. coli* elongation factor Tu bound to a GTP analogue displays an open conformation equivalent to the GDP-bound form. *Nucleic Acids Res.* 46:8641–8650.
21. Kavaliauskas, D., C. Chen, …, C. R. Knudsen. 2018. Structural dynamics of translation elongation factor Tu during aa-tRNA delivery to the ribosome. *Nucleic Acids Res.* 46:8651–8661.
22. Voorhees, R. M., T. M. Schmeing, …, V. Ramakrishnan. 2010. The mechanism for activation of GTP hydrolysis on the ribosome. *Science.* 330:835–838.
23. Wolf, H., G. Chinali, and A. Parmeggiani. 1977. Mechanism of the inhibition of protein synthesis by kirromycin. Role of elongation factor Tu and ribosomes. *Eur. J. Biochem.* 75:67–75.
24. Mesters, J. R., L. A. Zeef, …, L. Bosch. 1994. The structural and functional basis for the kirromycin resistance of mutant EF-Tu species in *Escherichia coli*. *EMBO J.* 13:4877–4885.
25. Schuette, J. C., F. V. Murphy, IV, …, C. M. Spahn. 2009. GTPase activation of elongation factor EF-Tu by the ribosome during decoding. *EMBO J.* 28:755–765.
26. Fischer, N., P. Neumann, …, H. Stark. 2015. Structure of the *E. coli* ribosome-EF-Tu complex at <3 Å resolution by Cs-corrected cryo-EM. *Nature.* 520:567–570.
27. Parmeggiani, A., and G. W. Swart. 1985. Mechanism of action of kirromycin-like antibiotics. *Annu. Rev. Microbiol.* 39:557–577.
28. Stark, H., M. V. Rodnina, …, M. van Heel. 1997. Visualization of elongation factor Tu on the *Escherichia coli* ribosome. *Nature.* 389:403–406.
29. Stark, H., M. V. Rodnina, …, M. van Heel. 2002. Ribosome interactions of aminoacyl-tRNA and elongation factor Tu in the codon-recognition complex. *Nat. Struct. Biol.* 9:849–854.
30. Valle, M., J. Sengupta, …, J. Frank. 2002. Cryo-EM reveals an active role for aminoacyl-tRNA in the accommodation process. *EMBO J.* 21:3557–3567.
31. Valle, M., A. Zavialov, …, J. Frank. 2003. Incorporation of aminoacyl-tRNA into the ribosome as seen by cryo-electron microscopy. *Nat. Struct. Biol.* 10:899–906.
32. Arenz, S., L. V. Bock, …, D. N. Wilson. 2016. A combined cryo-EM and molecular dynamics approach reveals the mechanism of ErmBL-mediated translation arrest. *Nat. Commun.* 7:12026.
33. Schwede, T., J. Kopp, …, M. C. Peitsch. 2003. SWISS-MODEL: an automated protein homology-modeling server. *Nucleic Acids Res.* 31:3381–3385.
34. Kjeldgaard, M., P. Nissen, …, J. Nyborg. 1993. The crystal structure of elongation factor EF-Tu from Thermus aquaticus in the GTP conformation. *Structure.* 1:35–50.
35. Pronk, S., S. Páll, …, E. Lindahl. 2013. GROMACS 4.5: a high-throughput and highly parallel open source molecular simulation toolkit. *Bioinformatics.* 29:845–854.
36. Hornak, V., R. Abel, …, C. Simmerling. 2006. Comparison of multiple Amber force fields and development of improved protein backbone parameters. *Proteins.* 65:712–725.
37. Poole, P. H., F. Sciortino, …, H. E. Stanley. 1992. Phase behaviour of metastable water. *Nature.* 360:324.
38. Joung, I. S., and T. E. Cheatham, III. 2008. Determination of alkali and halide monovalent ion parameters for use in explicitly solvated biomolecular simulations. *J. Phys. Chem. B.* 112:9020–9041.
39. Aduri, R., B. T. Psciuk, …, J. SantaLucia. 2007. AMBER force field parameters for the naturally occurring modified nucleosides in RNA. *J. Chem. Theory Comput.* 3:1464–1475.
40. Frisch, M. J., G. W. Trucks, …, D. J. Fox. 2009. Gaussian 09 Revision D.01. Gaussian Inc, Wallingford, CT.

41. Case, D., I. Ben-Shalom, …, P. Kollman. 2018. Amber 2018. University of California, San Francisco, CA.
42. Sousa da Silva, A. W., and W. F. Vranken. 2012. ACPYPE - AnteChamber PYthon Parser interfacE. *BMC Res. Notes.* 5:367.
43. Essmann, U., L. Perera, …, L. G. Pedersen. 1995. A smooth particle mesh Ewald method. *J. Chem. Phys.* 103:8577–8593.
44. Berendsen, H. J. C., J. P. Postma, …, J. R. Haak. 1984. Molecular dynamics with coupling to an external bath. *J. Chem. Phys.* 81:3684–3690.
45. Parrinello, M., and A. Rahman. 1981. Polymorphic transitions in single crystals: a new molecular dynamics method. *J. Appl. Phys.* 52:7182–7190.
46. Hess, B. 2008. P-LINCS: a parallel linear constraint solver for molecular simulation. *J. Chem. Theory Comput.* 4:116–122.
47. Feenstra, K. A., B. Hess, and H. J. C. Berendsen. 1999. Improving efficiency of large time-scale molecular dynamics simulations of hydrogen-rich systems. *J. Comput. Chem.* 20:786–798.
48. Bussi, G., D. Donadio, and M. Parrinello. 2007. Canonical sampling through velocity rescaling. *J. Chem. Phys.* 126:014101.
49. Amadei, A., A. B. Linssen, and H. J. Berendsen. 1993. Essential dynamics of proteins. *Proteins.* 17:412–425.
50. Roux, B. 1995. The calculation of the potential of mean force using computer simulations. *Comput. Phys. Commun.* 91:275–282.
51. Hub, J. S., B. L. De Groot, and D. Van Der Spoel. 2010. g_wham, A free weighted histogram analysis implementation including robust error and autocorrelation estimates. *J. Chem. Theory Comput.* 6:3713–3720.
52. Whitford, P. C., S. C. Blanchard, …, K. Y. Sanbonmatsu. 2013. Connecting the kinetics and energy landscape of tRNA translocation on the ribosome. *PLoS Comput. Biol.* 9:e1003003.
53. Michaud-Agrawal, N., E. J. Denning, …, O. Beckstein. 2011. MDAnalysis: a toolkit for the analysis of molecular dynamics simulations. *J. Comput. Chem.* 32:2319–2327.
54. Pingoud, A., W. Block, …, E. Fischer. 1982. The elongation factor Tu binds aminoacyl-tRNA in the presence of GDP. *J. Biol. Chem.* 257:11261–11267.
55. Janiak, F., V. A. Dell, …, A. E. Johnson. 1990. Fluorescence characterization of the interaction of various transfer RNA species with elongation factor Tu.GTP: evidence for a new functional role for elongation factor Tu in protein biosynthesis. *Biochemistry.* 29:4268–4277.
56. Parmeggiani, A., I. M. Krab, …, P. Nissen. 2006. Structural basis of the action of pulvomycin and GE2270 A on elongation factor Tu. *Biochemistry.* 45:6846–6857.
57. Dunkle, J. A., L. Wang, …, J. H. Cate. 2011. Structures of the bacterial ribosome in classical and hybrid states of tRNA binding. *Science.* 332:981–984.
58. Bock, L. V., C. Blau, …, H. Grubmüller. 2013. Energy barriers and driving forces in tRNA translocation through the ribosome. *Nat. Struct. Mol. Biol.* 20:1390–1396.
59. Bock, L. V., C. Blau, …, H. Grubmüller. 2015. Dynamic contact network between ribosomal subunits enables rapid large-scale rotation during spontaneous translocation. *Nucleic Acids Res.* 43:6747–6760.
60. Katava, M., M. Kalimeri, …, F. Sterpone. 2016. Stability and function at high temperature. What makes a thermophilic GTPase different from its mesophilic homologue. *J. Phys. Chem. B.* 120:2721–2730.
61. Chapman, S. J., J. M. Schrader, and O. C. Uhlenbeck. 2012. Histidine 66 in *Escherichia coli* elongation factor tu selectively stabilizes aminoacyl-tRNAs. *J. Biol. Chem.* 287:1229–1234.
62. Bock, L. V., M. H. Kolář, and H. Grubmüller. 2018. Molecular simulations of the ribosome and associated translation factors. *Curr. Opin. Struct. Biol.* 49:27–35.
63. Lai, J., Z. Ghaemi, and Z. Luthey-Schulten. 2017. The conformational change in elongation factor Tu involves separation of its domains. *Biochemistry.* 56:5972–5979.
64. Yang, H., J. Perrier, and P. C. Whitford. 2018. Disorder guides domain rearrangement in elongation factor Tu. *Proteins.* 86:1037–1046.
65. Yang, H., J. K. Noel, and P. C. Whitford. 2017. Anisotropic fluctuations in the ribosome determine tRNA kinetics. *J. Phys. Chem. B.* 121:10593–10601.
66. Vos, C., and P. Verwiel. 1973. Structure of the new antibiotic mocimycin (MYC 8003): chromophore and furopyranone fragment. *Tetrahedron Lett.* 14:2823–2826.
67. Maehr, H., M. Leach, …, J. F. Blount. 1980. The chemistry of aurodox and related antibiotics. *Can. J. Chem.* 58:501–526.
68. Dewey, R. S., B. H. Arison, …, G. Albers-Schönberg. 1985. The structure of efrotomycin. *J. Antibiot. (Tokyo).* 38:1691–1698.
69. Vogeley, L., G. J. Palm, …, R. Hilgenfeld. 2001. Conformational change of elongation factor Tu (EF-Tu) induced by antibiotic binding. Crystal structure of the complex between EF-Tu.GDP and aurodox. *J. Biol. Chem.* 276:17149–17155.
70. Parmeggiani, A., I. M. Krab, …, P. Nissen. 2006. Enacyloxin IIa pinpoints a binding pocket of elongation factor Tu for development of novel antibiotics. *J. Biol. Chem.* 281:2893–2900.
71. Parmeggiani, A., and P. Nissen. 2006. Elongation factor Tu-targeted antibiotics: four different structures, two mechanisms of action. *FEBS Lett.* 580:4576–4581.